# SEISMIC PERFORMANCE AND EFFECTS OF DIFFERENT JOINT SHAPES FOR UNBONDED PRECAST SEGMENTAL BRIDGE COLUMNS

**H.-L. Wang** * **S.-W. Liu** **Z. Zhang**

*The Institute of Bridge Engineering*
*Dalian University of Technology*
*Dalian, China*

## ABSTRACT

To study the seismic performance and the effects of different joint shapes for unbonded precast segmental bridge columns under low-reversed cyclic loading, two 3-D finite element (FE) models respectively using plane-contact joints and shear resistant joints were established. In the FE models, the mechanical behaviors of concrete and tendons were respectively described by the damage-plastic model and the bilinear model, and the contact criteria was based on Coulomb's Friction. The results of nonlinear time history analysis showed that the deformation of the columns was mainly composed of alternately open-closed joints, and the failure of the column was mainly caused by concrete crush on the bottom segment. Compared with two model's hysteresis loop, backbone curve, ductility and residual deformation, it was found that the column with shear resistant joints had longer stable period of strength, better ductility, and smaller residual displacement than the column with plane-contact joints, so it had better seismic performance.

**Keywords:** Precast segmental bridge column, Posttensioned strands, Hysteresis performance, Swing system.

## 1. INTRODUCTION

The use of the segmental technology for bridges has increased in recent years due to the advantages of short construction period, durability and little impact on traffic. Meanwhile precast segmental bridge column (PSBC) is becoming an important direction for the development of bridge engineering. It is found that rocking system is one way to achieve precast column. The segments of the column adopting swing system are connected by unbonded tendons, using alternately open-closed joints to improve seismic performance. The column using this approach can obtain the characteristics of precast erection, re-centering capability and destruction focused on the base of the column.

Researchers have done a lot of experiments and analysis on this construction method. Hewes and Priestley [1] did some pseudo-static tests about unbonded precast segmental bridge column (UPSBC) with steel tubular shell at the bottom of the segment, and did some analyses about the seismic performance under different depth-width ratio, thickness of the steel tube and tension stress. Tongji university bridge seismic discipline group [2,3] did a series of experiments to analyze the influences of seismic performance for PSBCs under different parameters, including presence of posttensioned (PT) strands, using unbonded or bonded tendons, number of segments, the assembling ways of segments and the distribution locations of PT strands, *etc*.. To overcome the disadvantages that energy dissipation (ED) is decreased while rocking the PSBC, some measures have been suggested, such as internal ED bars, external energy dissipaters, embedded elastomeric pads, and shear resistant connectors, *etc*. [4-10]. Concrete-filled fiber-reinforced polymer tubes, concrete-filled steel tubes, and fiber-RC composite have been used at the column-base area to avoid damage and to provide some ductility during earthquakes [9-15].

Based on the previous tests and researches, the seismic behaviors of UPSBC were evaluated by doing numerical simulation for 3-D finite element (FE) models under low-reversed cyclic loading in this study. Meanwhile, compared with plane-contact joint (PCJ), one type of shear resistant joint (SRJ) was put forward to discuss the influences of different joints of columns.

## 2. DESCRIPTION OF ANALYTICAL MODEL

Two FE models of UPSBCs were designed for simulating under lateral cyclic loading, designated as PCJ-UPSBC and SRJ-UPSBC. The structures of the two models were the same except of their joint shapes. PCJ were used in PCJ-UPSBC, and SRJ in SRJ-UPSBC. Both of them were 12 meters high, using rectangular

* Corresponding author (wanghuili@dlut.edu.cn)


DOI : 10.1017/jmech.2016.22
Copyright © 2016 The Society of Theoretical and Applied Mechanics
https://doi.org/10.1017/jmech.2016.22 Published online by Cambridge University Press

section of 2m by 2m, including a loading end and a fixed end respectively. The models consisted of concrete segments, reinforcement within the segments, unbonded tendons and rigid base. The concrete segments were connected by 8 root of 17$\phi_s$15.2 unbonded PT strands, which could produce pressure on the contact surfaces. Shear force was transmitted by static friction through segments. Lateral reciprocating displacement force was applied under a 1.2 × $10^4$kN constant compressive axial load to simulate the gravity load from bridge superstructures. The geometric details were shown in Fig. 1.

## 2.1 Constitutive Theories and Mesh

8-node, fully integrated, 3D linear continuum brick elements (C3D8) were used for modeling the concrete segments and foundation. The columns were meshed such that each element border length was approximately 40cm. 2-node linear 3-D truss elements (T3D2) were used to model the reinforcement within the segments and the PT strands with an approximate element length of 40cm. The FE models were shown in Fig. 2.

### 2.1.1 Concrete

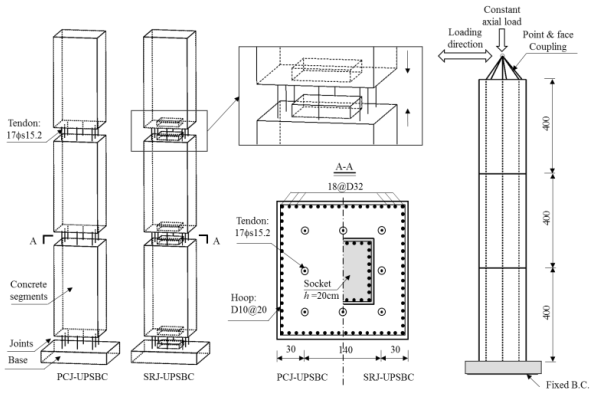
The concrete damage plasticity (CDP) model proposed by Lubliner, Lee and Fenve [16] was adopted because of its suitability to analyze cyclic loading and the capability to simulate hardness degradation and stiffness recovery under reverse loading. In CDP model, elastic stress-strain relationship was defined by the Young's modulus and ultimate elastic stress. A general constitutive relationship for CDP model was shown in Fig. 3, where $\varepsilon_{un}^{m}$ and $\sigma_{un}^{m}$ presents strain and stress of m-th tipping point, $\varepsilon_{pl}^{m}$ is concrete compressive plastic strain on m-th loading, $d_c$ is compressive damage factor, and $d_t$ is tensile damage factor. Hognestad proposed formula [17] was used to describe inelastic stress-strain curve, of which the upward section was parabola and the downward section was straight line. Compression section was defined as

$$\sigma=\begin{cases} f_c\left[2\dfrac{\varepsilon}{\varepsilon_0}-\left(\dfrac{\varepsilon}{\varepsilon_0}\right)^2\right] & \varepsilon\le\varepsilon_0 \\ f_c\left[1-0.15\dfrac{\varepsilon-\varepsilon_0}{\varepsilon_u-\varepsilon_0}\right] & \varepsilon_0\le\varepsilon\le\varepsilon_u \end{cases} \tag{1}$$

where $f_c$ = uniaxial compressive strength of concrete, $\varepsilon_0$ = yield strain, $\varepsilon_u$ = ultimate compressive strain. Tension section was defined as

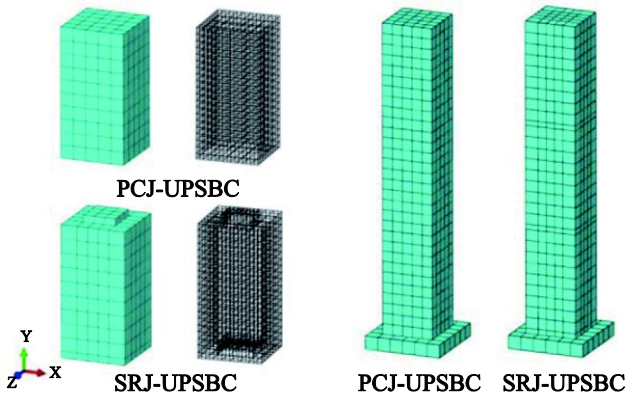
$$\sigma=f_t\frac{\dfrac{\varepsilon}{\varepsilon_t}}{a_t\left(\dfrac{\varepsilon}{\varepsilon_t}-1\right)^{1.7}+\dfrac{\varepsilon}{\varepsilon_t}} \qquad \varepsilon\ge\varepsilon_t \tag{2}$$

where $a_t=0.312f_t^2$, $f_t$ = uniaxial ultimate tensile stress of concrete, $\varepsilon_t$ = peak tensile strain of concrete.




(a) Joints and section (b) Boundary conditions and applied loads

Fig. 1 Geometric models.




(a) Concrete segment models (b) General FE models

Fig. 2 Details of the FE models.

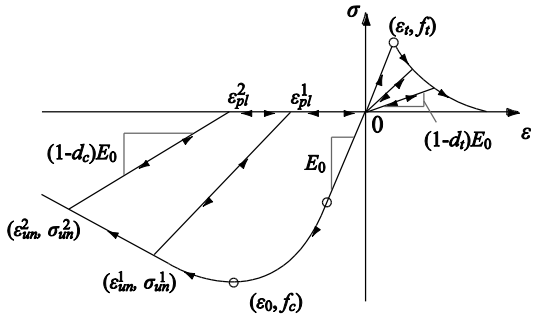



Fig. 3 Constitutive relationship for CDP model.

In this study, C30 concrete was adopted, where Young's modulus $E_0$ = 26.5GPa, uniaxial compressive strength $f_c$ = 30MPa, ultimate elastic compressive stress values 0.5$f_c$, uniaxial tensile strength $f_t$ = 1.78MPa. Uniaxial tensile and compressive stress-strain curve were shown in Figs. 4 and 5.

On the basis of the stress-strain relationship, material stiffness degradation under cyclic loading was considered by damage factor calculated according to the following formula [18]:

$$d_k=\frac{(1-\beta)\varepsilon_k^{in}E_0}{\sigma_k+(1-\beta)\,\varepsilon_k^{in}E_0}\ (k=t,c) \tag{3}$$



https://doi.org/10.1017/jmech.2016.22 Published online by Cambridge University Press

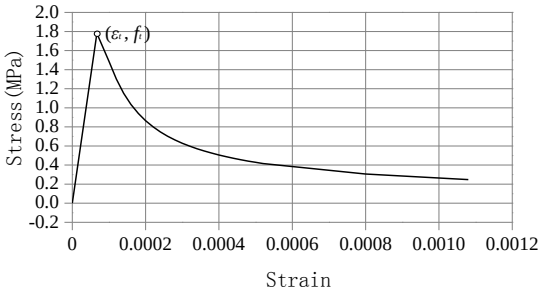



Fig. 4 Tensile stress-strain relationship under uniaxial stresses.

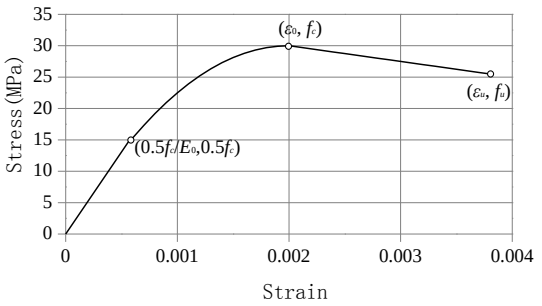



Fig. 5 Compressive stress-strain relationship under uniaxial stresses.

where $t$ and $c$ represent the tension and compression, $\beta$ is the proportion of plastic strain $\varepsilon_k^{pl}$ in inelastic strain $\varepsilon_k^{in}$. $\beta$ values 0.35 ~ 0.7 in compression and 0.5 ~ 0.95 in tension.

2.1.2 Reinforcement

Bilinear kinematic (BKIN) hardening of material was used to define the behavior of the steel bar, with VON MISES as yield criterion. Material properties for the bar were as follows: Elastic modulus $E_s$ = 200GPa; yield stress $f_y$ = 335MPa; yield strain $\varepsilon_y$ = 0.00168 and 0.1 $E_s$ as the slope of the hardening phase. Reloading stiffness under cyclic loading was evaluated by initial elastic stiffness. BKIN model for the steel bar behavior for unloading and reloading branches was shown in Fig. 6. The reinforcement cage was embedded in the concrete segment using an embedded region constraint type.

## 2.2 PT Strands

PT strands are necessary for segmental system. On one hand, normal pressure provided by tendons can increase critical friction between the contact surfaces to resist shear force. On the other hand, when a column has been deformed, it has the ability to restore the deformation with tendons. If the initial PT force is too high, plastic deformation will be produced in tendons during an earthquake resulting in loss of prestressing. If so, it cannot be guaranteed for seismic performance because of the decrease of the capacity to transfer shear and the increase of the residual displacement. Based on the above reasons, proper prestressing force should be adopted to ensure that it works in flexible states

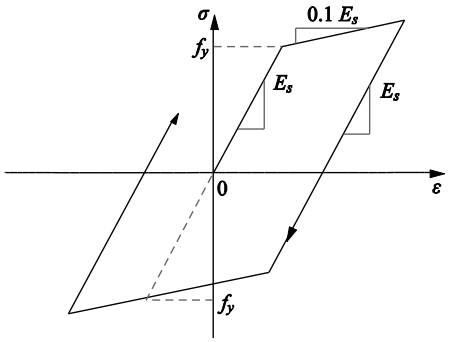



Fig. 6 Constitutive relationship for reinforcement.

during the earthquake. In this study, the mechanical model of the PT strands was also defined as BKIN model, where elastic ratio of prestressing tendons $E_s$ = 195GPa, yield stress $f_y$ = 1860MPa; yield strain $\varepsilon_y$ = 0.00954 and 0.1 $E_s$ as the slope of the hardening phase. Effective tensile stress $\sigma_{con}$ = 800MPa which was equivalent to 43% of the ultimate tensile strength, and axial compression ratio $u$ = 22.7%.

## 2.3 Boundary Conditions

As a cantilevered structure for pier, all degrees of freedom (DOF) should be constrained at the bottom of the column while all DOF at the top of the pier were unrestrained to simulate a free end. In order to obtain restraint forces conveniently, a reference point was coupled with the bottom surface of the foundation and the $U_x$, $U_y$, $U_z$, $R_x$, $R_y$ and $R_z$ DOF were constrained for it.

## 2.4 Behavior at Contact

When the concrete surfaces come into contact with each other, a contact algorithm is used to transmit stresses between the contacted surfaces. The used algorithm is a finite sliding formulation where separation and sliding of finite amplitude and arbitrary rotation of the surfaces may arise.

Shear stresses between two contacted surfaces are transmitted by the basic Coulomb friction model. The basic friction model assumes that the coefficient of friction $\mu$ is the same in all directions. For a three-dimensional simulation there are two orthogonal components of shear stress, $\tau_1$ and $\tau_2$, along the interface between the two bodies. The two shear stress components are combined into an "equivalent shear stress," $\bar{\tau}$, for the stick/slip calculations, where

$$\bar{\tau} = \sqrt{\tau_1^2 + \tau_2^2} \tag{4}$$

A two-dimensional representation for the stick/slip calculations was shown in Fig. 7 [18]. The normal direction of the contact algorithm is defined using hard contact. Penalty function method is used as the contact formulation, which is solved by using the Full Newton iteration method. For tangential components of the contacted surfaces, coefficient of friction valued 0.2 [4].



https://doi.org/10.1017/jmech.2016.22 Published online by Cambridge University Press

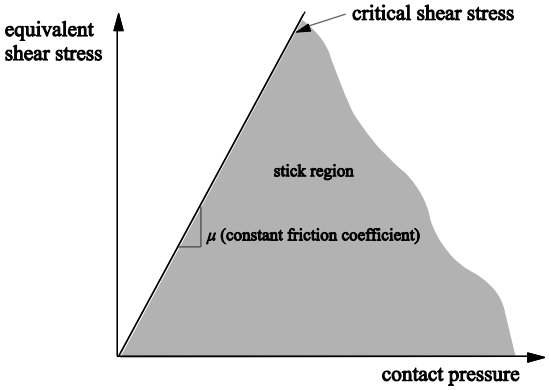



Fig. 7 A two-dimensional representation for the stick/slip calculations.

### 2.5 Model Loading

Loading for both of the columns was a two-step process. First, a $1.2 \times 10^4$kN constant compressive axial load was applied at the top of the column; meanwhile a prestressing force was imposed by shortening of 800MPa for each of the PT strands. Then, a lateral low-reversed cyclic load in a displacement control was applied for the nonlinear time-history analysis to get load-displacement relationship for the models. Displacement-time curve was shown in Fig. 8 with the maximum of 500mm.

## 3. ANALYTICAL STUDY

### 3.1 Mode of Deformation and Failure

The deformation of the column under positive loading and negative loading was shown in Fig. 9. A large joint opening at the base of the column can be clearly seen. The lateral deformation is mainly caused by the reciprocation rotation of the bottom concrete segment around the foundation. During positive loading, the left side of the bottom joint is open while the right side is closed. During negative loading, the left side is closed and the right side is open. It shows that the model of the joint alternately opening and closing is consistent with the actual situation.

Lateral slip over time of the two models given in Fig. 10 shows that the amount of slip fluctuate up and down near the origin and the maximum values 4mm, which is much smaller than the element length. Therefore, it can be considered that there is no lateral shift between the segments when concrete coefficient of friction values 0.2.

The result of compressive damage (DAMAGEC) for PCJ-UPSBC and SRJ-UPSBC (Shown in Fig. 11) represents the value of concrete compressive damage variable $d_c$ in the models. Obviously, the area of the damage mainly appears in the bottom segment. The calculated results show that post-tensioning bars are still in elastic state (Shown in Fig. 12), so the failure mode is concrete crush on the foot of the column.

### 3.2 Hysteretic Behavior

Hysteresis curve is effective to reflect the seismic performance of the structure. The load-displacement

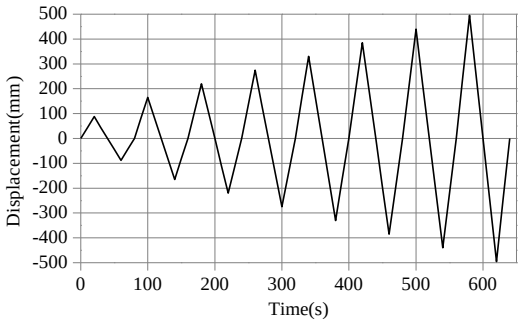



Fig. 8 Lateral displacement-time relationship for loading.

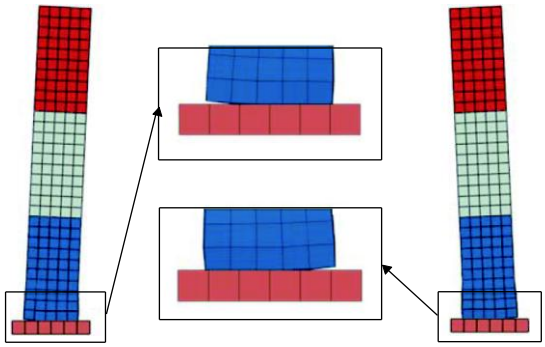


Fig. 9 Forward and reverse deformation of the models.

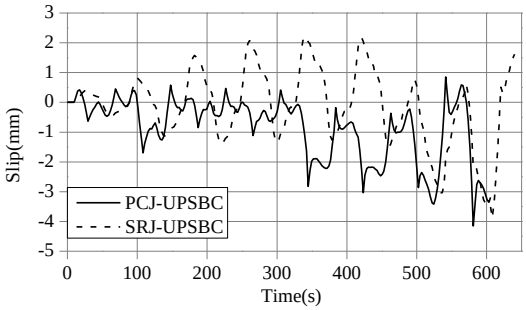



Fig. 10 Horizontal slip-time relationship for the bottom joints.

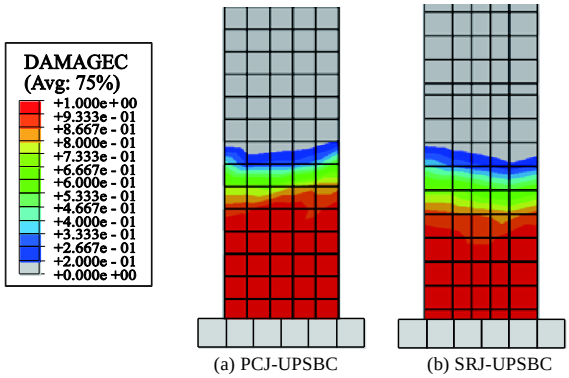



Fig. 11 Percentage of concrete plastic damage for the models.



https://doi.org/10.1017/jmech.2016.22 Published online by Cambridge University Press

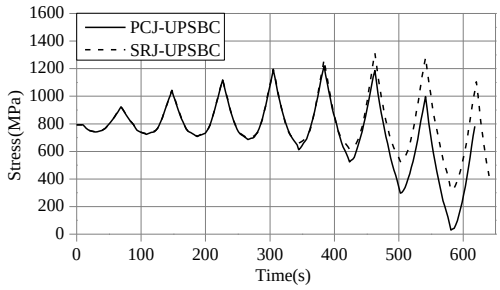



Fig. 12 Stress variation of PT strands.

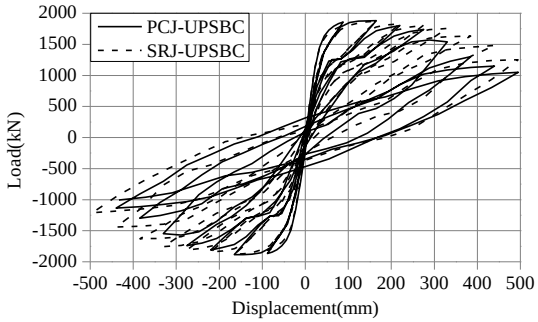



Fig. 13 Lateral load-displacement hysteretic relationship.

hysteresis curve for PCJ-UPSBC and SRJ-UPSBC was given in Fig. 13. It can be seen from the curve that the hysteresis loops for both of the models are shuttle-shaped and elongated. Moreover, Hysteretic energy dissipation was shown in Fig. 14. The energy dissipation of PCJ-UPSBC is a little greater than SRJ-UPSBC, which means energy-dissipating capacity of PCJ-UPSBC is basically same as SRJ-UPSBC.

### 3.3 Backbone Curve

Backbone curve is obtained by linking peak points under the first loop of the same lateral displacement on the hysteresis curve. Strength, deformation, ductility and some other aseismatic indexes are clearly reflected by the backbone curve shown in Fig. 15. As known in the figure, under small lateral force, the analysis shows a linear response of the columns. Both of the models have the same maximal bearing capacity. Nevertheless, compared with PCJ-UPSBC, SRJ-UPSBC has longer stabilization stage of the strength.

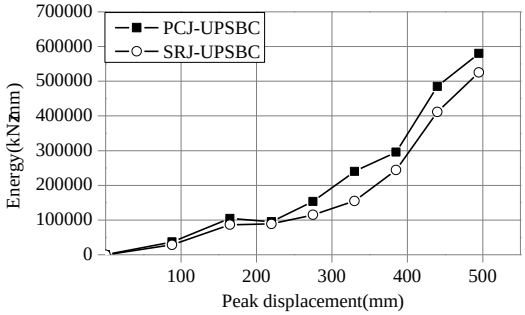



Fig. 14 Hysteretic energy dissipation.

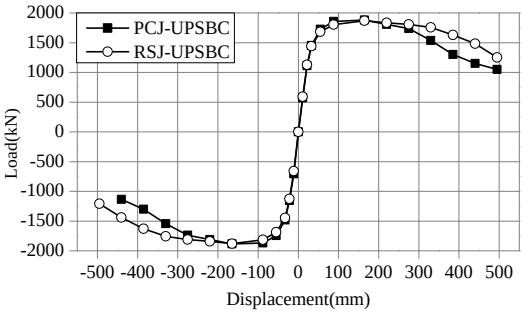



Fig. 15 Backbone curves.

### 3.4 Ductility

Ductility is the capacity of inelastic deformation before the initial strength occurs obvious deterioration. It is a sign of seismic performance for the columns and it is measured by ductility coefficient $\mu_m$:

$$\mu_m = \frac{U_m}{U_y} \tag{5}$$

where $U_m$ = maximum drift, which is the horizontal displacement when the lateral bearing capacity of the pier drop to 85% of maximum; $U_y$ = yield drift, which is equivalent to the displacement on° top of the pier when longitudinal reinforcement in the concrete segments first yield. The ductility coefficients of the two models were listed on Table 1. It can be seen that the ductility of SRJ-UPSBC is better than PCJ-UPSBC.

Table 1 Characteristic displacement and displacement ductility factor.

| Model | $U_y$ (mm) | $U_m$ (mm) | $\mu_m$ |
|---|---|---|---|
| PCJ-UPSBC | 66 | 314.0 | 4.76 |
| SRJ-UPSBC | 66 | 397.6 | 6.02 |

### 3.5 Residual Deformation

The residual deformation refers to the irreversible plastic deformation for the column after unloading. If only small residual deformation is occurred, the column may be still working after the earthquake and it will be benefit for repairing to reduce economic losses. Therefore, the residual deformation is the most important embodiment of seismic performance.

To eliminate the influence of component height, residual angle $\theta_{residual}$ was used to express residual displacement:

$$\theta_{residual} = \frac{\Delta}{L} \tag{6}$$

where $\Delta$ = The horizontal residual displacement; $L$ = column height. $\theta_{residual}$-$\mu$ curve for the models was shown in Fig. 16. $\mu$ presents ductility index, which is the radio of $U_y$ to peak displacement of each hysteresis loop. Compared with the proportion standing at 80%



https://doi.org/10.1017/jmech.2016.22 Published online by Cambridge University Press

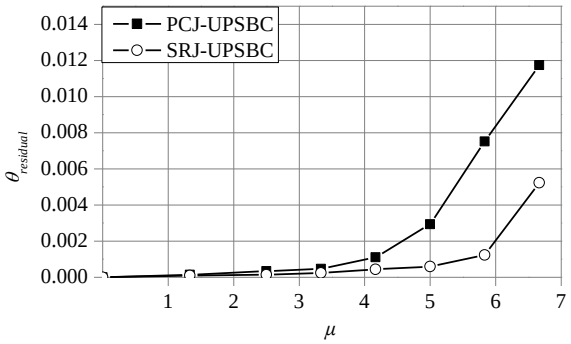



Fig. 16 $\theta_{residual}$-$\mu$ relationship

for reinforced concrete column, the residual displacement only accounts for 30% of the total displacement for PSBC, which means PSBC has a good re-centering capability. Moreover, it can be seen that the residual displacement of SRJ-UPSBC is always smaller than PCJ-UPSBC at the same $\mu$ within their ultimate states. Therefore, the re-centering capability of SRJ-UPSBC is stronger than PCJ-UPSBC.

## 4. CONCLUSIONS

This study investigated the seismic performance of UPSBCs with different type of joints. From the results of the numerical simulations, the following conclusions were reached.

1. The degradation of stiffness, strength for the columns and the appearance of the bottom joints with alternately open-close state were simulated well, which meant the results of the two three-dimensional FE models conformed to the mechanical performance of the actual structures.
2. When the coefficient of friction values 0.2, no slip occurs between the segments of the precast columns. The lateral deformation of the column is mainly composed of alternately open-closed joints. The PT strands always work within the elastic range. The failure of the column is mainly caused by the concrete crush on the bottom segment.
3. The column with PCJs and with SRJs have the same lateral bearing capacity, but the column with SRJs has longer stable period of strength, better ductility, and smaller residual displacement than the column with PCJs, so it has better seismic performance.

## ACKNOWLEDGEMENTS

This work was supported by China Scholarship Council [grant number 201506060044]; the State Key Laboratory of Structural Analysis for Industrial Equipment, Dalian University of Technology [grant number S13209]; the Liaoning Provincial Department of Education [grant number L2014027]; the Fundamental Research Funds for the Central Universities [grant number DUT15QY34].

## REFERENCES

1. Hewes, J. T. and Priestley, M. J. N., "Seismic Design and Performance of Precast Concrete Segmental Bridge Columns," M.S. Thesis, Department of Civil Engineering, University of California, San Diego, U.S.A. (2002).
2. Wang, Z. Q., Song, W., Wang, Y. Y. and Wei, H. Y., "Numerical Analytical Model for Seismic Behavior of Prestressing Concrete Bridge Column Systems," *Procedia Engineering*, **14**, pp. 2333–2340 (2011).
3. Wang, Z. Q., Ge, J. P. and Wei, H. Y., "Seismic Performance of Precast Hollow Bridge Piers with Different Construction Details," *Frontiers of Structural and Civil Engineering*, **8**, pp. 399–413 (2014).
4. Chou, C. C. and Chen, Y. C., "Cyclic Tests of Post- Tensioned Precast CFT Segmental Bridge Columns with Unbonded Strands," *Earthquake Engineering & Structural Dynamics*, **35**, pp. 159–175(2006).
5. Palermo, A., Pampanin, S. and Marriott D., "Design, Modeling, and Experimental Response of Seismic Resistant Bridge Piers with Posttensioned Dissipating Connections," *Journal of Structural Engineering*, **131**, pp. 1648–1661 (2007).
6. Wang, J. C., Ou, Y. C., Chang, K. C. and Lee, G. C., "Large-Scale Seismic Tests of Tall Concrete Bridge Columns with Precast Segmental Construction," *Earthquake Engineering & Structural Dynamics*, **37**, pp. 1449–1465 (2008).
7. Motaref, S., Saiidi, M. S. and Sanders, D., "Shake Table Studies of Energy-Dissipating Segmental Bridge Columns," *Journal of Bridge Engineering*, pp. 186–199 (2014).
8. Kim, T. H., Lee, H. M., Kim, Y. J. and Shin, H. M., "Performance Assessment of Precast Concret Segmental Bridge Columns with a Shear Resistant Connecting Structure," *Engineering Structures*, **32**, pp. 1292–1303 (2010).
9. ElGawady, M. A., Booker, A. J. and Dawood, H. M., "Seismic Behavior of Posttensioned Oncrete-Filled Fiber Tubes," *Journal of Composites for Construction*, pp. 616–628 (2010).
10. ElGawady, M. A. and Sha'lan, A., "Seismic Behavior of Self-Centering Precast Segmental Bridge Ents," *Journal of Bridge Engineering*, pp. 328–339 (2011).
11. Youm, K. S., Cho, J. Y., Lee, Y. H. and Kim, J. J., "Seismic Performance of Modular Columns Made of Concrete Filled FRP Tubes," *Engineering Structures*, **57**, pp. 37–50 (2013).
12. Nikabakht, E., Rashid, K., Hejazi, F., Osman, S. A. and Mohseni, I., "Nonlinear Finite Element Analysis of PC Segmental Bridge Columns Subjected to Quasi-Static Loading," *International Journal of Advancements Civil Structural and Environmental Engineering*, **1**, pp. 28–31 (2013).
13. Dawood, H., ElGawady, M. and Hewes, J., "Behav ior of Segmental Precast Posttensioned Bridge Piers Under Lateral Loads," *Journal of Bridge Engineer-*



https://doi.org/10.1017/jmech.2016.22 Published online by Cambridge University Press

*ing*, pp. 735–746 (2012).

14. Motaref, S., Saiidi, M. S. and Sanders, D., "Shake Table Studies of Energy-Dissipating Segmental Bridge Columns," *Journal of Bridge Engineering*, pp. 186–199 (2014).
15. Trono, W., Jen, G., Panagiotou, M., Schoettler, M. and Ostergag, C. P., "Seismic Response of a Damage-Resistant Recentering Posttensioned-HYFRC Bridge Column," *Journal of Bridge Engineering*, 10.1061/(ASCE)BE.1943-5592.0000692 (2014).
16. Lee, J. and Fenves, G. L., "Plastic-Damage Model for Cyclic Loading of Concrete Structures," *Journal of Engineering Mechanics*, **124**, pp. 892–900 (1998).
17. Hognestad, E., "Study of Combined Bending and Axial Load in Reinforced Concrete Members," Technical Reports, College of Engineering, University of Illinois at Urbana Champaign (1951).
18. Zhang, G. L. and Su J., "Nonlinearity Analysis of Reinforced Concrete Based on ABAQUS," *Technology and Engineering*, 20, pp. 5620–5624 (2008).

(Manuscript received May 25, 2015,
accepted for publication December 21, 2015.)



https://doi.org/10.1017/jmech.2016.22 Published online by Cambridge University Press